



Optimization of Spraying Process and Laser Treatment of CoNiCrAlY

E. Lugscheider, D. Hofmann, and A.R. Nicoll

This article describes the investigation of a new generation of vacuum plasma sprayed CoNiCrAlY coatings on NiCr20Ti in the sprayed as well as the laser-treated condition. The aim of the study was the improvement of MCrAlY coating properties by modifying the microstructure through laser remelting with 5-kW Co₂ lasers. Parameter analysis and optimization was carried out for the vacuum plasma spraying process, as well as for the laser remelting technique. The effect of the laser treatment on microstructure, quality of the coatings, and oxidation as well as hot gas corrosion behavior are reported.

1. Introduction

MCrAlY alloys are used widely in gas turbine blades for protection against hot gas erosion and corrosion. Turbine blades are manufactured from either cast MCrAlY alloys or from MCrAlY coated nickel superalloys.

The CoNiCrAlY coatings on NiCr20Ti (Nimonic 75) base material examined in this study were manufactured by a two-step process consisting of vacuum plasma spraying of MCrAlY powder and the subsequent laser treatment of these coatings. It was anticipated that the established oxidation behavior, hot gas corrosion, and erosion properties of the laser remelted layers would be improved due to modification of the microstructure.^[1-3] Laser treatment is used to remelt specific areas of coated turbine blades.

2. Vacuum Plasma Spraying of CoNiCrAlY

MCrAlY alloys must be plasma sprayed in vacuum or within a low-pressure inert atmosphere to prevent oxidation of powder particles and the coating surface during spraying. Nimonic 75 was chosen as the substrate material (70 by 50 by 10 mm), because it is widely used for this purpose. Table 1 gives the composition of the CoNiCrAlY alloy and Nimonic 75 used in this study. The particle size of the atomized CoNiCrAlY powder was - 400 mesh.

The microstructure of sprayed coatings is influenced by numerous process parameters. Published results^[4-7] indicate that chamber pressure, current, spraying distance, and H₂ content of the plasma gas have the most important effect on the degree of melting of the powder particles, thickness and porosity of coatings, and surface roughness. Most of these coating properties have an effect on the absorption of laser radiation.

First, it is necessary to determine the complex interactions and correlation between spraying parameters and microstructure

to ensure development of optimum coating properties for subsequent laser treatment, which result in optimized laser remelted zones. Data on the effect of spraying parameters on microstructure can be obtained by using a factorial two-level experiment. It is based on a statistically optimized test plan that quantifies individual actions and interactions of all parameters with minimized experimental effect.^[4,8-10] In the present case, the investigation was performed by an 2⁴ factorial plan. The spraying parameters are given in Table 2.

To ensure statistical significance, every parameter set was carried out three times in random order. Additionally, zero-level tests were performed to verify reproducibility and to check the linearity of the regression equations. Laser treatment thickness and porosity of the coatings were selected as target variables.

The samples were manufactured using vacuum plasma spraying equipment made by Plasma-Technik AG. The substrate material was blasted with corundum, cleaned by recombination cleaning (sputtering) with an transferred arc, and preheated to 800 to 900 °C to exceed the ductile-brittle transition temperature of this type of MCrAlY alloy.^[11] Preheating MCrAlY alloys is necessary to prevent cracks during cooling after spraying^[12] and to increase adhesion between the substrate and the coating. A typical temperature history measured during the coating process by thermocouples at the substrate/coating interface is shown in Fig. 1.

A summary of the thickness, porosity, roughness, and microhardness of the sprayed coatings is given in Table 3. The specified values of coating thickness refer to a single-layer coating.

Table 1 Composition of MCrAlY Powder and Base Material

Alloy	Composition, wt. %						
	Co	Ni	Cr	Al	Y	Fe	Ti
CoNiCrAlY alloy....	36.7	32.6	21.2	8.9	0.6	<0.15	...
Nimonic 75.....	...	75	19.5	5	0.4

Table 2 Spraying Parameters

Chamber pressure, mbar	100 ± 40
Intensity of current, A.....	650 ± 70
H ₂ content, SLPM	8 ± 3
Spraying distance, mm.....	320 ± 50

Key Words: CoNiCrAlY coating, element distribution, hot corrosion tests, laser treatment, vacuum plasma spraying

E. Lugscheider and **D. Hofmann**, Material Science Institute, Aachen University of Technology, Aachen, Germany; and **A.R. Nicoll**, Plasma-Technik AG, Wohlen, Switzerland.

All measurements of thickness and porosity were taken into account for a regression analysis to determine the significant effects of these variables on microstructure. Roughness and microhardness had no significant effect in the chosen parameter field. Although porosity is measurable, but is not effected significantly by varying spraying parameters, coating thickness is greatly affected by the current intensity and hydrogen content of the plasma gas mixture. Furthermore, the interaction of current intensity and spraying distance is significant. The effects of varying the spraying parameters are presented in Table 4.

The negative effect of the regression coefficient with respect to the current intensity and hydrogen content indicates that coating thickness decreases when these factors are increased. This effect suggests that the optimum plasma energy is close to or below the lowest level examined. Optimization of these factors is attained when each change causes a decrease in coating thickness. Use of plasma energy greater than optimum leads to increased vaporization of smaller powder particles, which in this case cannot contribute to layer formation. This is confirmed by comparison of coating morphologies manufactured by counter-current parameter sets of current intensity, chamber pressure,

and spraying distance. As shown in Fig. 2(a), a homogenous fine-grained morphology with no unmelted particles is achieved with high plasma energy (correlated to high current intensity and high hydrogen content) as well as with a low spraying distance. The opposite parameter set (Fig. 2b) leads to a distinct lamellar morphology, characterized by partially doughy and not completely molten powder particles.

In addition to these primary effects, there is an underlying two-factor interaction of current and spraying distance. If both

Table 3 Results of Factorial Two-Level Experiments

Coating thickness, μm	245 to 380
Coating porosity, %	0.2 to 0.7
Surface roughness	
R_a , μm	3.7 to 4.5
R_z , μm	24 to 27.5
Microhardness, HV 0.05 kg	510 to 590

Note: R_a is the arithmetic average of the surface profile. R_z is the maximum roughness between the highest and lowest regions of the surface.

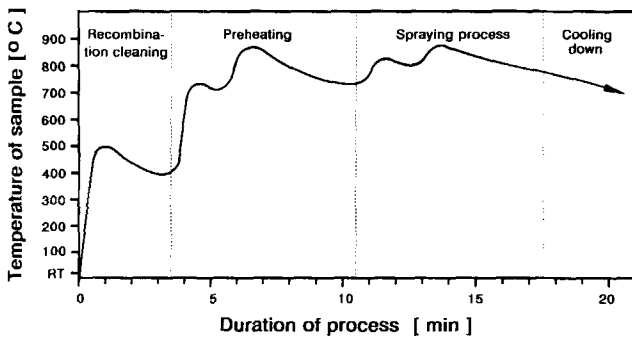
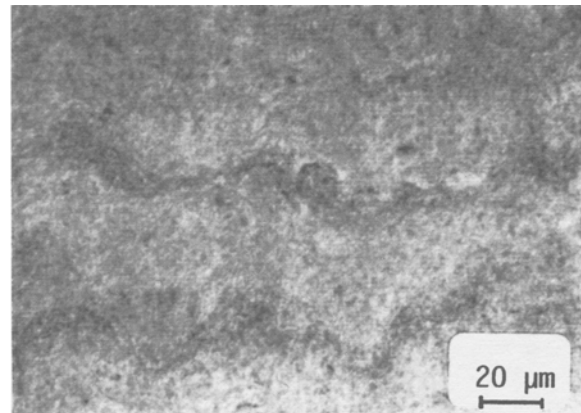
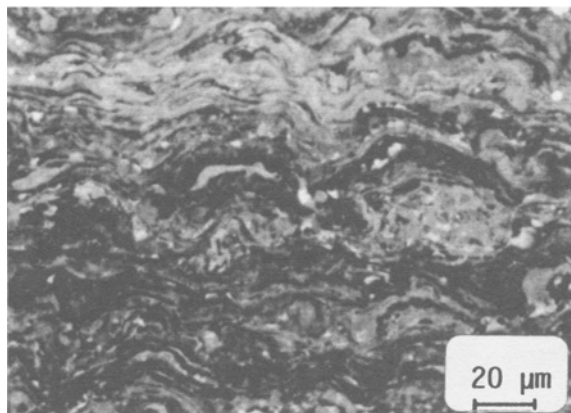


Figure 1 Course of sample temperature during the coating process.

Table 4 Effects of Varying Spraying Parameters on Thickness and Porosity of Coatings

Spraying parameter	Coating thickness	Porosity of coatings
Intensity of current.....	Decreasing	No significant effect
H ₂ content.....	Decreasing	No significant effect
Spraying distance.....	No significant effect (Decreasing)	No significant effect
Chamber pressure.....	No significant effect (Increasing)	No significant effect
Intensity of current combined with spraying distance.....	Increasing	No significant effect



580 A.....	Intensity of current	720 A
140 mbar.....	Chamber pressure	60 mbar
11 SLPM.....	Hydrogen content	11 SLPM
370 mm.....	Spraying distance	270 mm

Figure 2 Microstructures of vacuum plasma sprayed CoNiCrAlY coatings as a result of extremely different spraying parameter sets. The table shows the corresponding spray parameters that were used.

primary effects are negative, then the influence of the first variable decreases when the second variable is increased. For this reason, the influence of current intensity on coating thickness is greater at low spraying distances than at high levels. The reverse of this relation is also valid for spraying distance, but spraying distance, as a primary factor, was not significant. In spite of this, in the case of varied spraying distance, a change in the effect of current intensity was taken into account.

The determined regression equations allow, within the stated parameter field, the exact regulation of coating properties, which are significant in terms of laser posttreatment. In the present study, only coating thickness and not porosity, is significantly affected by spraying parameters. The investigated interactions do not completely correspond with the results of a CoCrAlY alloy published by Dekumbis *et al.*,^[4] which can be explained by a different parameter field and use of an MCrAlY alloy with a modified composition. Figure 3 shows the microstructure of a nonetched and etched double layer CoNiCrAlY coating, illustrating low porosity in the nonetched condition and the typical structure with some inserted nonfused powder particles after etching.

In practice, vacuum plasma sprayed MCrAlY coatings undergo heat treatment before use in gas turbines. In the present case, heat treatment consisted of two steps: first 2 h at 1120 °C in vacuum and second 24 h at 840 °C in air. The microstructure of this heat treated CoNiCrAlY coatings is shown in Fig. 4, revealing a distinct diffusion zone between the coating and substrate, as well as grain growth and a change in phase composition. After heat treatment, a cobalt-rich Co-Ni-Cr matrix with a low aluminum content and a β NiAl phase with cobalt and a low chromium concentration can be found within the sprayed coatings.

Electron probe microanalysis (EPMA) is showed extremely small yttrium-rich precipitates containing nearly 10 wt.% yttrium. The nickel content in the diffusion zone increased significantly, which is related to the nickel base element of the substrate material. Contrary to the matrix composition mentioned above, the chromium content decreased whereas the aluminum, iron, and of course the nickel concentration increased in this matrix. A network of high chromium regions existed at the diffusion zone and at the upper region of the substrate material. An accumulation of very fine-grained yttrium-rich phases was also detected.

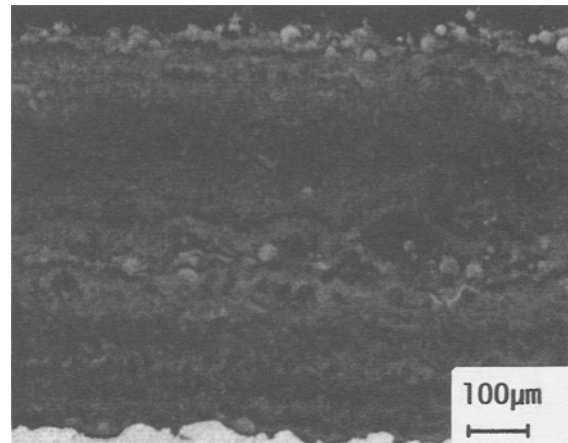
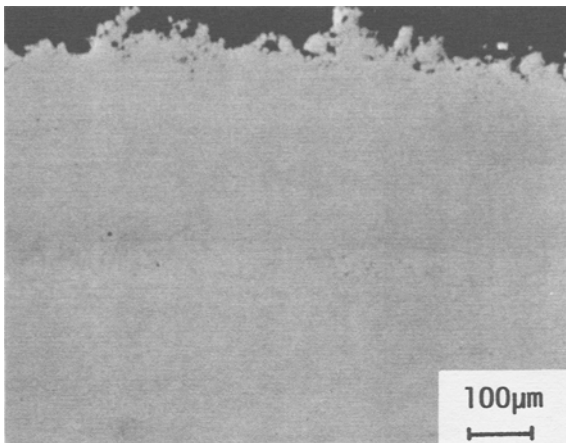


Figure 3 Vacuum plasma sprayed double-layer CoNiCrAlY coating in the nonetched (a) and etched (b) conditions.

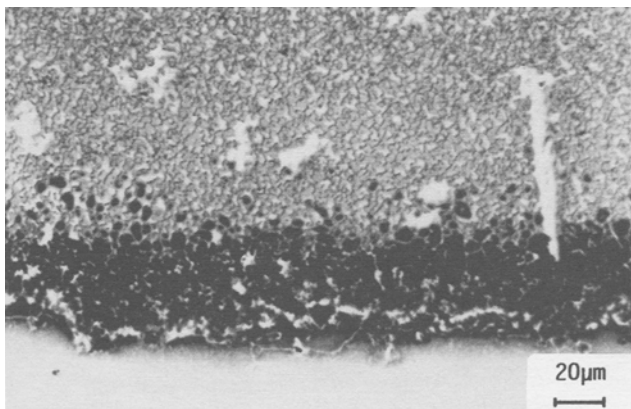


Figure 4 Microstructure of heat treated CoNiCrAlY coating with a distinct diffusion zone.

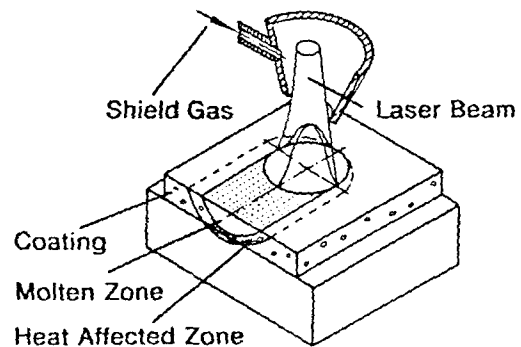
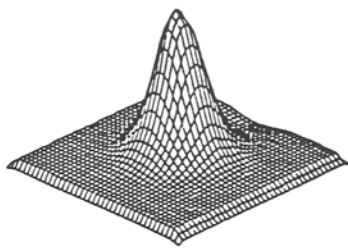
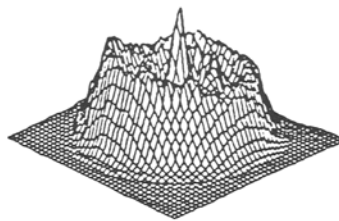


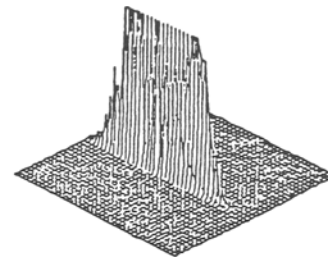
Figure 5 Two-step laser process.^[13]



Rofin-Sinar RS 5000
Gaussian-mode
parabolic mirror
 $r_B = 1$ mm defocused
 $P_L = 0,05 - 1,5$ kW



Rofin Sinar RS 5000
Donut-mode
parabolic mirror
 $r_B = 3$ mm defocused
 $P_L = 1 - 5$ kW



Heraeus C76
Rectangular Gaussian-mode
linefocus
 $6 \times 0,2$ mm
 $P_L = 1 - 5$ kW

Rofin-Sinar RS 5000
Gaussian mode
parabolic mirror
 $r_B = 1$ mm defocused
 $P_L = 0.05$ to 1.5 kW

Rofin Sinar RS 5000
Donut mode
parabolic mirror
 $r_B = 3$ mm defocused
 $P_L = 1$ to 5 kW

Heraeus C76
Rectangular Gaussian mode
line focus
 6×0.2 mm
 $P_L = 1$ to 5 kW

Figure 6 Beam forms and operational data of CO_2 lasers used in this study (by ILT and IPT, Aachen).

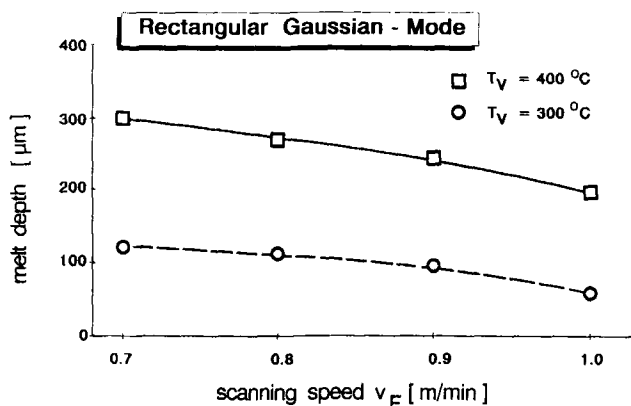


Figure 7 Melt depth versus scanning speed related to different preheating temperatures ($P_L = 1.5$ kW; coating thickness, $300 \mu\text{m}$).

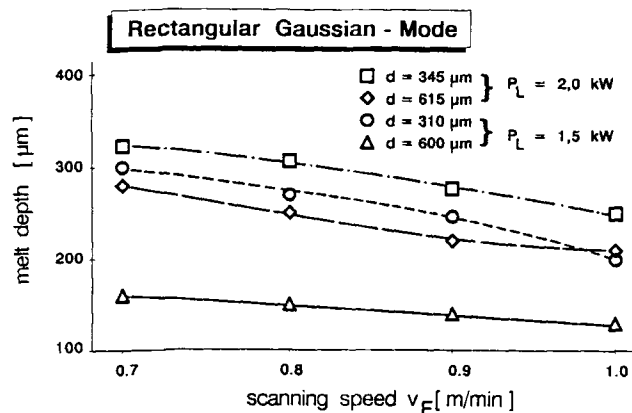


Figure 8 Melt depth versus scanning speed related to different coating thicknesses and laser powers.

Furthermore, a characteristic square or needle-shaped phase was present, with considerable chromium (~88 wt.%) and low cobalt, nickel, and aluminum concentrations in the center of these phases. On the other hand, at the interface of these phases, an element concentration similar to the nickel-rich Ni-Co-Al phase (β NiAl) can be noted. Subsequent laser treatment was normally performed on coatings in the as-sprayed condition.

3. Laser Surface Fusion of CoNiCrAlY Coatings

To fulfill the desired demand of improved oxidation and hot gas/corrosion behavior, plasma sprayed CoNiCrAlY coatings

are laser beam fused as close as possible to the substrate material. Melting of the substrate should be avoided to prevent element dilution. Figure 5 illustrates the two-step process of laser surface treatment.

Continuous-wave CO_2 lasers, with a power range of 1 to 5 kW but different laser modes, beam forms, and energy distributions, were used for the remelting experiments (Fig. 6). The quality of laser-remelted CoNiCrAlY coatings depends on the laser power (P_L), scanning speed (v_F), preheating temperature, and coating morphology, such as coating thickness and porosity. The influence of a sprayed coating porosity of 2.0% and above leads to an increased formation of gas bubbles within the laser-fused zone. The expanding gas within the pores inside the overheated melt are not able to rise to the surface and dissipate. The scan-

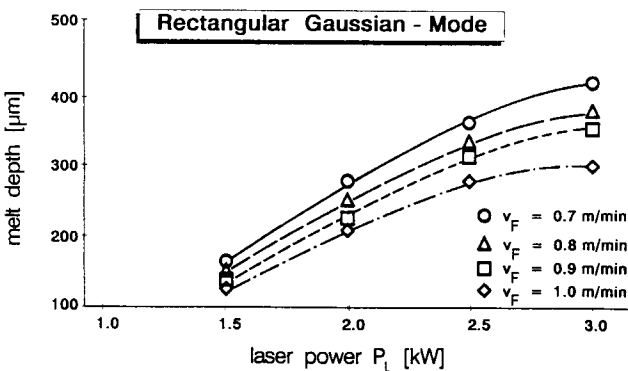
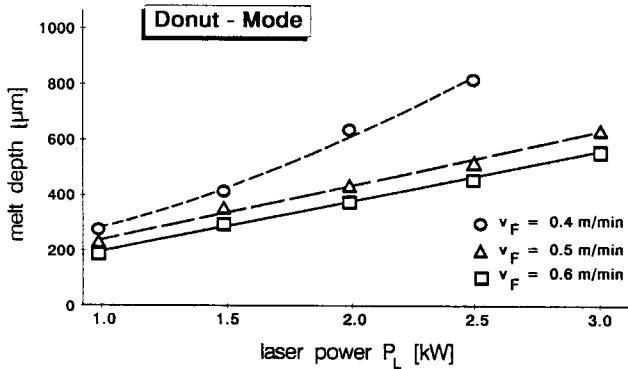
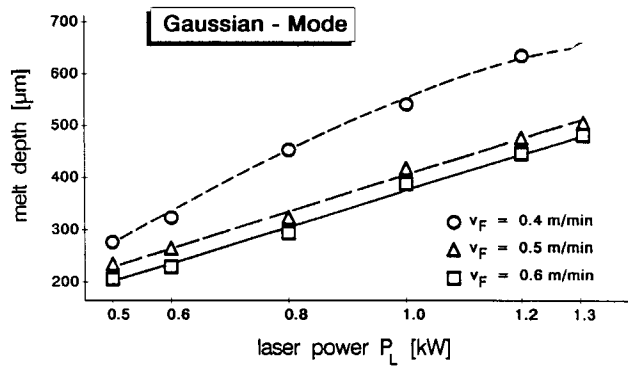


Figure 9 Melt depth versus different laser modes as a function of laser power and scanning speed (uniform coating thickness 600 to 700 μm).

ning speed, which determines the life of the melt, cannot be further reduced. However, as mentioned above, CoNiCrAlY vacuum plasma sprayed coatings can be plasma sprayed with less than 1% porosity; therefore, porosity of the coating does not influence the laser treatment.

The coatings were preheated to 400 to 450 $^{\circ}\text{C}$ before starting laser treatment to reduce sensitivity to cracking, which occurs when the line focus of the Heraeus laser is used. Argon was used as a shielding gas to prevent oxidation of the melting pool and the area surrounding the laser track during the laser process. The relationship of preheating temperature to melt depth under identical conditions in terms of coating morphology and laser treat-

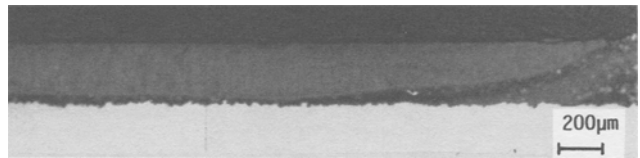


Figure 10 Cross section of Gaussian mode laser track at single-layer CoNiCrAlY coating of $\sim 300 \mu\text{m}$ thickness before heat treatment.

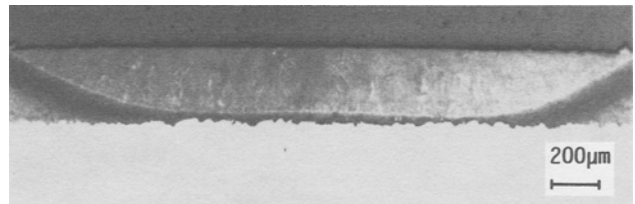


Figure 11 Cross section of Gaussian mode laser track at single-layer CoNiCrAlY coating of $\sim 300 \mu\text{m}$ thickness before heat treatment.

Table 5 EDX Phase Analysis Before and After Heat Treatment for Gaussian Mode Laser Track and As-Sprayed and Heat Treated Conditions

Condition	Matrix	Composition, wt. %				
		Co	Ni	Cr	Al	Y
Vacuum plasma sprayed coating						
After heat treatment	βNiAl	43.4	28.9	24.2	3.4	...
		22.2	52.8	5.4	21.4	...
Laser track						
Before heat treatment	βNiAl	37.8	32.6	21.1	8.1	0.4
		32.1	35.9	16.5	14.8	0.7
After heat treatment	βNiAl	43.1	27.7	25.5	3.7	...
		22.5	51.6	7.4	18.8	...

ment parameters is illustrated in Fig. 7. Increasing the preheating temperature leads to an increase in melt depth.

The relationship between melt depth and coating thickness is shown in Fig. 8. Under identical process conditions, coatings with large thickness are laser fused much deeper than coatings of smaller thickness due to the different thermophysical properties of the substrate and coating material (e.g., thermal conductivity), as well as the effect of heat transfer coefficient, which leads (depending on coating thickness) to heat stagnation and partial reflection at the coating/substrate interface.

Figure 9 shows the results of the melting experiments, in which the laser power of the three modes and scanning speed of the laser beams were varied. Contrary to the results of phase formation, reported by Bhat *et al.*,^[14] yttrium segregation at the interface between the coating and the laser treated zone was not detected, but yttrium-rich phases with high aluminum content

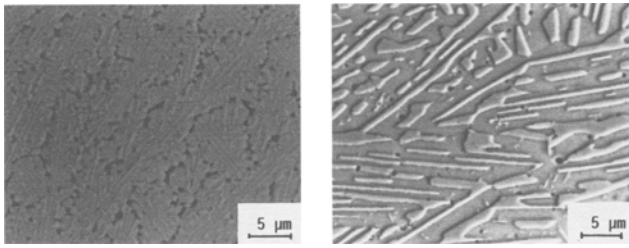


Figure 12 Phase formation before and after heat treatment for the Gaussian mode.

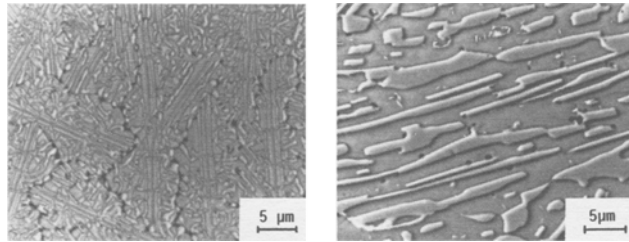


Figure 13 Phase formation before and after heat treatment for the Donut mode.

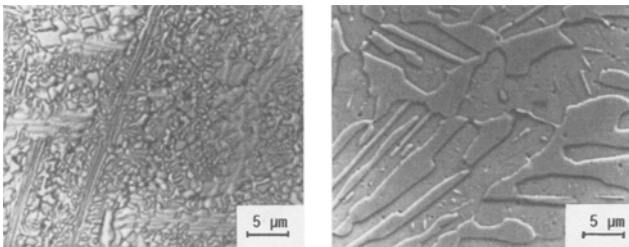


Figure 14 Phase formation before and after heat treatment for the rectangular Gaussian mode line with the focused Heraeus C76-laser.

were found at the surface of the laser-fused zone. Following the thesis of Nowok,^[15] these precipitates form the nuclei for clusters of keying or pegging alumina scale.

Complete cross sections of laser-fused tracks, manufactured with a Rofin Sinar RS 5000 Laser used in the Gaussian mode and a Heraeus C 76 laser used in the rectangular Gaussian mode at similar coating thickness, are presented in Fig. 10 and 11. These figures exhibit extremely different fusion zone geometries, but in all cases a crack-free and completely dense microstructure without pores was produced.

After the laser treatment, the specimens were heat treated in the same manner as coatings in the as-sprayed condition mentioned above. Heat treatment caused an increase in phases and variation in phase composition. These differences are shown in Table 5 (*e.g.*, Gaussian mode). The other laser modes yield the same effects, including phase composition changes, after heat treatment. For both conditions (*i.e.*, as-sprayed or sprayed and

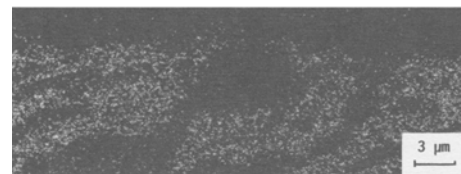
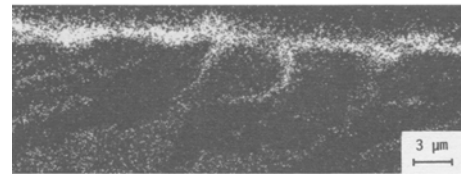
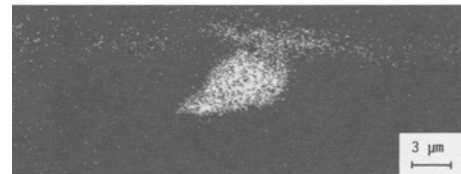
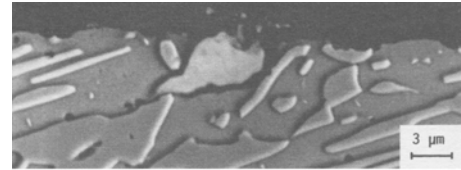


Figure 15 Yttrium-rich precipitates at the surface of the laser track after heat treatment. X-ray distribution maps of yttrium, aluminum, and chromium are presented. (a) Yttrium-rich phase at the surface. (b) Yttrium distribution. (c) Aluminum distribution. (d) Chromium distribution.

laser fused), the composition after heat treatment of the two primary phases was found to be very similar. Figures 12 to 14 show the phase that developed after heat treatment, as well as the identical morphology, which does not depend on the different laser modes and diverse intensity distributions.

The formation of yttrium-rich precipitates at the surface was verified by scanning electron microscopy (SEM) (Fig. 15) and X-ray distribution maps of yttrium, aluminum, and chromium. The phase analysis of the yttrium distribution for this CoNi-CrAlY alloy generally corresponds to the data of Smeggil *et al.*^[16] for a laser-fused CoCrAlY coating, but disagrees with results of Liu *et al.*^[17] for a laser-clad CoCrAlY alloy with a diluted substrate material.

The effect of the laser fusion process, as well as heat treatment, on hardness is shown in Fig. 16. Clearly, the laser remelting process causes a decrease in hardness, which is enhanced by heat treatment. These effects are caused by changes in phase composition and grain size, inhomogeneities along the grain boundaries, as well as residual stresses.

The roughness of laser-remelted CoNiCrAlY-vacuum plasma sprayed coatings manufactured by the three different laser modes and at least seven overlapped laser tracks is summarized in Table 6, which examines a laser-glazed surface of high quality with minimal subsequent post treatment.

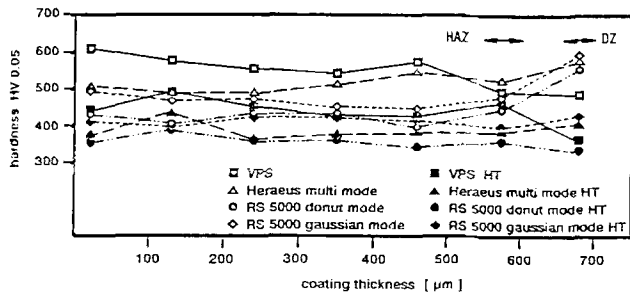


Figure 16 Influence of laser melting and heat treatment on hardness profiles of CoNiCrAlY coatings.

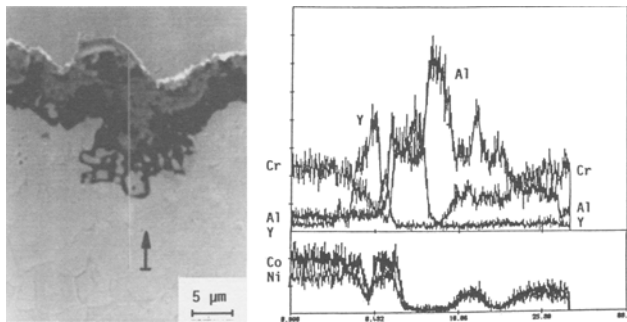


Figure 17 SEM/EDX line scan of oxide surface layer of a vacuum plasma sprayed coating in the as-sprayed condition after oxidation tests.

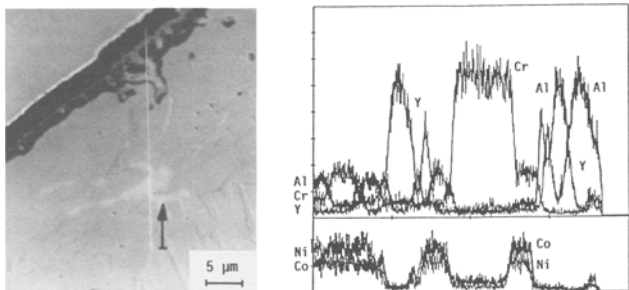


Figure 18 SEM/EDX line scan of surface layer zone of laser-fused and non-heat-treated CoNiCrAlY coating after oxidation tests.

4. Oxidation and Hot Gas Corrosion of Vacuum Plasma Sprayed CoNiCrAlY Coatings

Oxidation and hot gas corrosion tests were conducted for six possible material conditions: as sprayed; sprayed and laser fused; sprayed and heat treated; sprayed, heat treated, and laser fused; sprayed, laser fused, and heat treated; and sprayed, heat treated, laser fused, and heat treated.

Compared with coatings in the as-sprayed or sprayed and heat treated condition, oxidation tests carried out for 100 h at

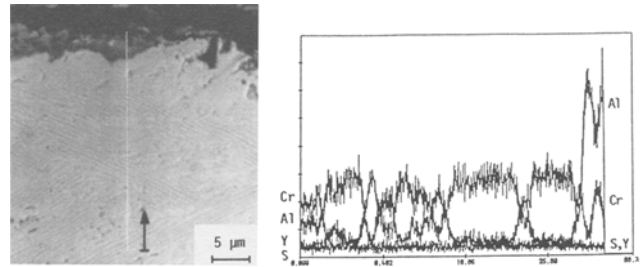


Figure 19 SEM/EDX line scan providing element distribution of the corroded zone and regions near the surface of a laser-fused, non-heat-treated vacuum sprayed coating.

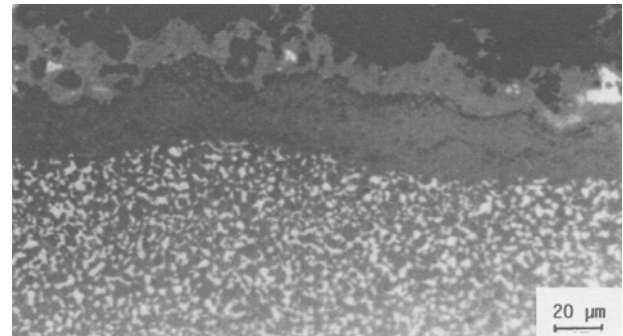


Figure 20 Microstructure of hot gas corroded sprayed and heat treated CoNiCrAlY coating.

Table 6 Comparison of Surface Roughness Before and After Laser Treatment

Roughness, μm	Sprayed coating	Heraeus C76		
		rectangular Gaussian mode	RS5000 Donut mode	RS 5000 Gaussian mode
R_a	3.7 to 4.5	0.4 to 0.9	0.6 to 2.0	0.4 to 2.0
R_z	22.0 to 28.0	2.7 to 7.1	4.7 to 14.2	2.0 to 13.9

1050 °C in air showed the best results for laser-fused CoNiCrAlY coatings. These coatings, in either the as-received or heat treated condition, exhibited dense, thin oxide scales with good adhesion characteristics, which when combined with a very small zone impoverished of oxide-forming elements (reservoir phases) gave an indication of improved life. Figures 17 and 18 illustrate the differences in the oxide scales that formed and clearly show the keying or pegging effect (Fig. 18) of mixed alumina and yttria scales. A significant influence of heat treatment on the oxidation behavior of laser-remelted CoNiCrAlY vacuum plasma sprayed coatings was not stated. These results agree in general with several published results concerning different MCrAlY systems and distinct laser surface treatments.^[2,3,14,16,17]

In addition to oxidation tests, the hot gas corrosion behavior of the six different material conditions was tested in an artificial slag and synthetic air containing 0.03 vol% SO₂ for 300 h at 950

°C. The composition of artificial slag was 4.3 wt.% Na₂SO₄, 22.7 wt.% CaSO₄, 2 wt.% H₂O, 22.3 wt.% Fe₂O₃, 20.6 wt.% ZnSO₄ · H₂O, 10.4 wt.% K₂SO₄, 2.8 wt.% MgO, 6.5 wt.% Al₂O₃, and 10.4 wt.% SiO₂. These test conditions correspond to those of hot gas corrosion type I, also called sulfidation, which is characterized by basic fluxing reactions that form aggressive low-melting salts that penetrate and destroy the protective coating.

The results of hot gas corrosion tests agree with the oxidation test results mentioned above. Independent of heat treatment, laser-fused CoNiCrAlY coatings formed a thin, dense scale with good adhesion combined with a very small zone free of oxide scale-forming elements. As shown in the EDX line scan (Fig. 19) of the surface zones, there is no sulfur penetration. An EDX analysis of the corroded surface layer on a laser-fused CoNiCrAlY coating shows primarily the presence of nickel, aluminum, zinc, chromium, iron, silicon, and cobalt. In contrast to the results of laser-treated coatings that indicate improved life, Fig. 20 is a micrograph of a corroded sprayed and heat treated coating that exhibits an extensive impoverished zone of oxide scale-forming elements. Laser remelting of plasma sprayed CoNiCrAlY coatings leads to the anticipation of an improved life for laser-treated coatings compared to conventional as-sprayed and heat treated coatings.

After oxidation or hot gas corrosion tests, porosity at the diffusion zones between the coating and substrate, as well as at oxide scale surface layers in the case of non-laser-treated coatings, is attributed to the Kirkendall effect.^[14,18,19]

5. Conclusions

The interactions between spraying process parameters and the resulting morphology of CoNiCrAlY coatings are discussed and analyzed by a factorial two-level experiment. Based on these results an optimized microstructure for laser remelting related to thickness and porosity as well as the accompanying process parameters was developed. Single or overlapped multi-track laser remelting of optimized coatings using three different laser modes led to very dense, fine-grained, and crack-free laser tracks, provided workpieces were preheated to 400 °C. The results of laser remelting with the various modes, related to phase formation before and after heat treatment, were nearly identical and exhibit a primarily Ni-Co-Cr matrix, with βNiAl as the reservoir phase of oxide forming-elements, as well as extremely small yttrium-rich precipitates. Compared to coatings in the as-sprayed condition, laser-treated coatings exhibit improved oxidation and hot gas corrosion resistance. Properties do not depend on subsequent heat treatment as is usually the case for MCrAlY materials.


Acknowledgments

This article is based on a project that was financially supported by the German Bundesminister für Forschung und Technologie (BMFT). Special thanks are directed to the Fraunhofer Institut für Lasertechnik (ILT) and the Fraunhofer Institut für Produktionstechnologie (IPT), Aachen, Germany, for assistance

with laser processing. The authors are responsible for the content of the paper.

References

1. D.H. Boone, W.D. Goward and P.G. Moore, "Structure of Laser-Treated MCrAlY Coatings," paper presented at the International Conference on Metallurgical Coatings, San Francisco, Apr 6-10 (1981).
2. H. Bhat, R.A. Zatorski, H. Herman and R.J. Coyle, "Laser Treatment of Plasma-Sprayed Coatings," *10th Int. Thermal Spraying Conf.*, Essen, DVS-Berichte, Vol 80, 21-23 (1983).
3. W. Weitoa, R. Streiff, and W. Maocai, "Effect of Laser Surface Modification on High Temperature Oxidation Behavior of Alloys and Coatings," *J. Mater. Sci. Eng. A*, 121, 499-507 (1989).
4. R. Dekumbis, P. Huber and M. Villat, "MCrAlY Vacuum Plasma-Sprayed Coatings: Factorial Two-Level Experiments as an Aid to Determine the Influence of Spraying Parameters on Coating Properties," *10th Int. Thermal Spraying Conf.*, Essen, DVS-Berichte, Vol 80, 153-161 (1983).
5. O. Meunier, Ch. Coddet, and P. Huber, "Study of the Effect of a Superimposed Transferred Arc during Plasma-Spraying of MCrAlY-Powders," *Thermal Spraying Conf. TS 90*, Essen, DVS-Berichte, Vol 130, 19-22 (1990).
6. P. Mazars and D. Manesse, "Influence of Low Pressure Plasma-Spraying Parameters on the Microstructure of MCrAlY-Deposits. Coatings for Heat Engines," Proc. 1st NATO Advanced Workshop on Coatings for Heat Engines, Acquafredda di Maratea, Italy, 579-593 (1984).
7. P. Huber, R. Dekumbis, and M. Villat, "Vacuum Plasma Sprayed CoCrAlY: Influence of Spraying Parameters and Heat Treatment on Structure," Proc. 15th Int. Congress on Combustion Engines, Paris, 579-596 (1983).
8. E. Lugscheider, D. Hofmann, D. Schubert and A.R. Nicoll, "Application of Two-Level Factor Analysis to the Optimization of Thermal Spray Coatings Using the Example of Plasma Spraying," *J. Schweißen Schneiden*, 43,(10), 217-219 (1991).
9. E. Scheffler, Einführung in die Praxis der statistischen Versuchsplanung., VEB-Verlag für Grundstoffindustrie, Leipzig (1974).
10. G.E.P. Box, W.G. Hunter, and J.S. Hunter, *Statistics for Experimenters*, John Wiley & Sons, (1978).
11. M.I. Wood, "Mechanical Interactions between Coatings and Super-alloys under Conditions of Fatigue," *J. Surf. Coat. Technol.*, 39/40, 29-42 (1989).
12. K. Schneider and H.W. Grünling, "Mechanical Aspects of High Temperature Coatings," *Thin Solid Films*, 107, 395-416 (1983).
13. E. Lugscheider, D. Hofmann, F. Jansen, A.R. Nicoll, E.W. Kreutz, K. Wissenbach and A. Gasser, "Improvement of the Properties of Vacuum-Plasma-Sprayed Titanium Layers by Laser Densification," 3rd European Conference on Laser Treatment of Materials (ECLAT), Erlangen, 523-533 (1990).
14. H. Bhat, H. Herman, and R.J. Coyle, "Laser-Treated Plasma-Sprayed Ni-Base Alloy Coatings," Proc. 112th AIME Annual Meeting, Atlanta, 7-8 Mar 1983, in *High Temperature Protective Coatings*, 37-50.
15. J. Nowok, "Formation Mechanism of Keying or Pegging Yttrium Oxide and Increased Plasticity of Alumina Scale on FeCrAlY," *J. Oxidation Met.*, 18, H 1/2, 1-17 (1982).
16. J.G. Smeggil, A.W. Funkenbusch, and N.S. Bornstein, "The Effects of Laser Surface Processing on the Thermally Grown Oxide Scale Formed on a Ni-Cr-Al-Y Composition," *Thin Solid Films*, 119, 327-335 (1984).

- 
17. C.A. Liu, M.J. Humphries, and R.C. Krutenat, "Production of Fe-Cr-Al-Y and Co-Cr-Al-Y Coatings by Laser Surface Fusion and Their Oxidation Behavior," *Thin Solid Films*, 107, 269-275 (1983).
 18. E.Y. Lee, D.M. Chartier, R.R. Biederman, and R.D. Sisson, Jr., "Modelling the Microstructural Evolution and Degradation of M-Cr-Al-Y-Coatings During High Temperature Oxidation," *Surf. Coat. Technol.*, 32, 19-39 (1987).
 19. J.A. Nesbitt, Ph.D. thesis, Michigan Technical University, NASA TM-83738 (1984).